Signal processing in microwave-induced thermoacoustic tomography

Yuan Xu, Lihong V. Wang

Yuan Xu, Lihong V. Wang, "Signal processing in microwave-induced thermoacoustic tomography," Proc. SPIE 4256, Biomedical Optoacoustics II, (15 June 2001); doi: 10.1117/12.429294

SPIE.

Event: BiOS 2001 The International Symposium on Biomedical Optics, 2001, San Jose, CA, United States

Signal processing in microwave-induced thermoacoustic tomography

Yuan Xu, Lihong V. Wang*
Optical Imaging Laboratory, Biomedical Engineering Program
Texas A&M University, 3120 TAMU, College Station, Texas 77843-3120

* Author to whom all correspondence should be addressed. Telephone: 979-847-9040; fax: 979-845-4450; electronic mail: LWang@tamu.edu; URL: http://oilab.tamu.edu.

ABSTRACT

Microwave-induced thermoacoustic tomography was explored to image biological tissues. Short microwave pulses irradiated tissues to generate acoustic waves by thermoelastic expansion. The microwave-induced thermoacoustic waves were detected with a focused ultrasonic transducer to obtain two-dimensional tomographic images of biological tissues. The dependence of the axial and the lateral resolutions on the spectra of the signals was studied. A self-adaptive filter was applied to the temporal piezoelectric signals from the transducer to increase the weight of the high-frequency components, which improved the lateral resolution, and to broaden the spectrum of the signal, which enhanced the axial resolution.

Keywords: microwave, ultrasonics, thermoacoustics, tomography, resolution, filter

1. INTRODUCTION

When electromagnetic radiation is absorbed in biological tissues, the heating and the subsequent expansion will cause emission of acoustic signals, which is called the thermoacoustic effect. In thermoacoustic tomography, the thermoacoustic signals from a tissue sample are collected to map the distribution of the radiative absorption within the sample. The radiative absorption is closely related to the physiological and pathological status of the tissue: for example, cancerous breast tissues are 2–5 times more strongly absorbing to microwaves than surrounding normal breast tissues, which has been attributed to an increase in bound water and sodium within malignant cells.[1–3]

Thermoacoustic tomography combines good imaging resolution with good imaging contrast. Purely microwave imaging has the advantage of good imaging contrast but suffers from poor spatial resolution due to the large wavelength of microwaves.[4–7] On the other hand, purely ultrasonic imaging has good spatial resolution but poor contrast. Thermoacoustic tomography can bridge the gap between them.

There are various types of thermoacoustic tomography, such as photoacoustic tomography and microwave-induced thermoacoustic tomography (MITT). In photoacoustic tomography,[8–10] due to the use of short laser pulses—several nanoseconds in pulse width—and the strong attenuation of the laser light by tissues, the frequency spectrum of the acoustic signal from the buried object of several micrometers in size is estimated to have significant components up to 75 MHz,[9] which makes its axial resolution as good as 10 μm. However, the maximum imaging depth in photoacoustic tomography is limited by the strong attenuation of the laser light and of the high-frequency acoustic waves. On the other hand, MITT can be used to image much deeper tissues due to the relatively low absorption of microwaves. The spectra of the acoustic signals in MITT are usually below 2 MHz, and the axial resolution is greater than 1 mm. Several investigators employed microwave-induced thermoacoustic waves in the 1980s for imaging of biological tissues; these early works however did not produce any tomographic or depth-resolved images.[11–13] Recent progress realized tomographic imaging of biological tissues based on microwave-induced thermoacoustic waves.[14–17]

We here present our studies on the signal-processing aspect of scanning MITT. In our imaging approach, the lateral resolution was achieved by use of a focused ultrasonic transducer, whereas the axial resolution was obtained by measuring the temporal profiles of the acoustic signals. The dominance of the low-frequency (<0.5 MHz) components in the raw temporal signals limited the lateral resolution, and the narrow bandwidth of the signals restricted the axial resolution. A self-adaptive filter was applied to the temporal signals from the transducer to increase the weight of the high-frequency components, which improved the lateral resolution, and to broaden the spectrum of the signal, which enhanced the axial resolution.

Biomedical Optoacoustics II, Alexander A. Oraevsky, Editor,
Proceedings of SPIE Vol. 4256 (2001) © 2001 SPIE · 1605-7422/01/$15.00

2. METHODS

The experimental setup for this study is shown in Fig. 1. A Cartesian coordinate system was set up for reference: the *x* axis pointed outward perpendicularly to the drawing plane, the *y* axis pointed to the right in the drawing plane, and the *z* axis pointed upward along the acoustic axis. A 3-GHz microwave generator transmitted microwave pulses. The pulse width was modified from the original manufacturer's setting to 0.5 μs. A function generator was employed to trigger the microwave generator, to control its pulse repetition frequency, and to synchronize the sampling by the oscilloscope. Microwave energy was delivered by a tapered waveguide with a cross section that gradually narrowed from 72 mm × 34 mm to 72 mm × 5 mm. The object to be imaged was a slab of chicken muscle with a *y*-*z* cross section of 14 mm × 8 mm, and the slab was plunged into lard contained in a plexiglass tank. The tank was mounted on a two-dimensional (2-D) *x*-*y* translation stage (MD2, Arrick Robotics), which was driven by two computer-controlled stepper motors. Lard and plexiglass were used for their low absorption to microwaves. Lard also provided good acoustic coupling to an ultrasonic transducer facing the microwave waveguide. The central frequency of the ultrasonic transducer (V314, Panametrics) was 1 MHz, the bandwidth was 0.6 MHz, the diameter of the active element was 1.9 cm, and the focal length was 2.5 cm. The transducer was connected to a low-noise pulse preamplifier. The amplified signal was averaged 100 times, recorded by an oscilloscope (TDS-640A, Tektronix), and then transferred to a personal computer.

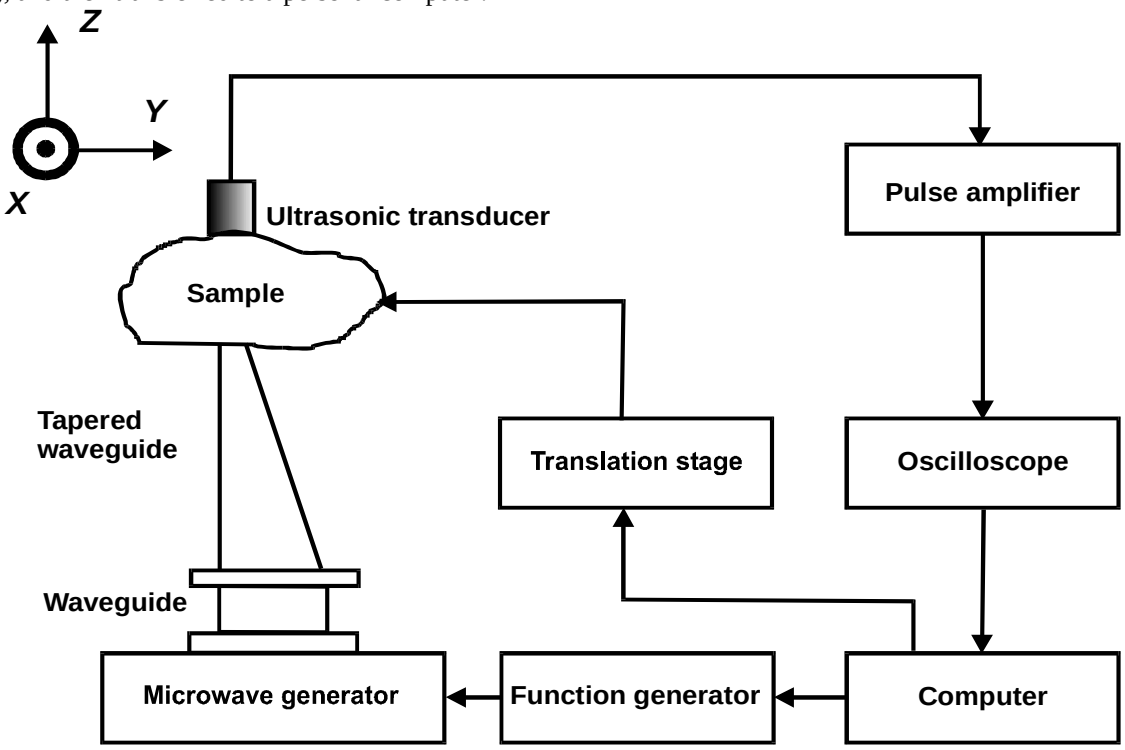

Fig. 1. Experimental setup for scanning MITT.

In our scanning MITT, the ultrasonic transducer measured the time-of-arrival signals of the thermoacoustic waves. The distances between the thermoacoustic sources and the transducer were calculated by multiplying the time of arrival with the speed of sound in the medium. Therefore, a time-domain signal can be converted into a one-dimensional (1-D) image along the acoustic axis (*z* axis), which is similar to an ultrasonic A-scan image. Scanning the sample along the *x* or the *y* axis and combining the multiple 1-D images yielded a 2-D cross-sectional image of the sample in the *x*-*z* or *y*-*z* plane, which is analogous to an ultrasonic B-scan image.

3. RESULTS AND DISCUSSION

An image of the chicken muscle is presented in Fig. 2(a). Each vertical line in this 2-D image was obtained from a temporal piezoelectric signal of the ultrasonic transducer, and the sample was scanned horizontally along the *y* axis with a step size of 1 mm to acquire the multiple vertical lines. Figures 2(b) shows the frequency spectra, respectively, for *y* equal to 20 mm—where the transducer axis crossed the muscle—and equal to 2 mm—where the transducer axis did not cross the muscle. The buried muscle was clearly imaged as shown in Fig. 2(a): the white line at z = 17 mm corresponds to the upper boundary

between the lard and the muscle, and the dark line at z = 25.1 mm to the lower one. The thickness of the muscle in the image is 8.1 mm and agrees with the actual one. But the lateral resolution is poor: the width of the muscle in the image appears to be 36 mm, much greater than the actual 14-mm width. Furthermore, there appear many ghost objects between the two boundaries and below the lower boundary. Because the muscle and the lard are almost uniform, no heterogeneity in the image is expected from other than the boundaries.

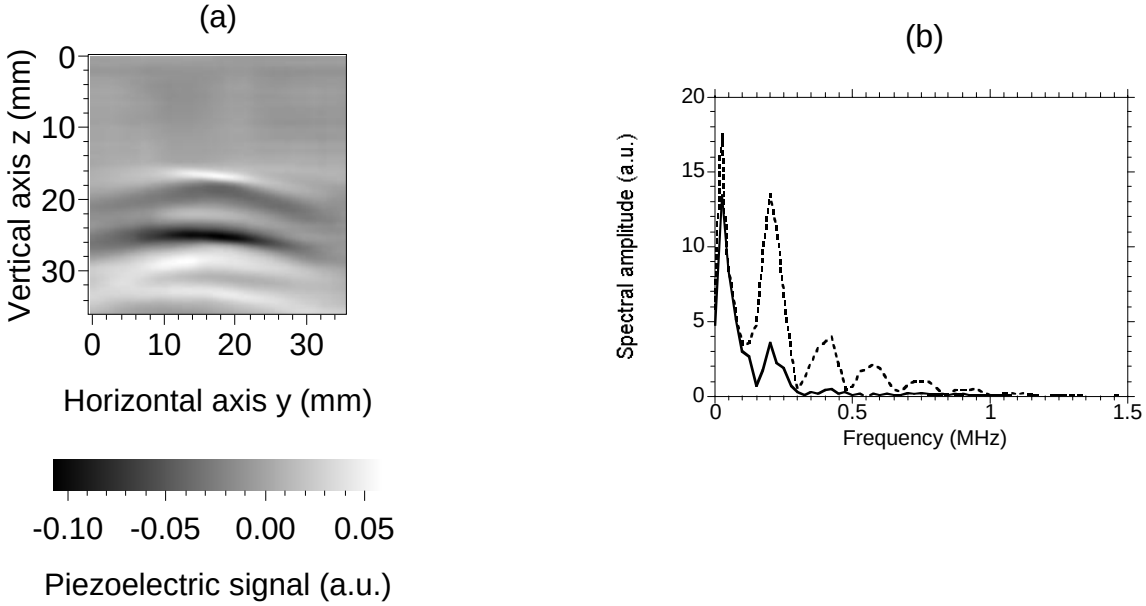

Fig. 2. (a) 2-D image of the *y*-*z* cross section of the sample obtained by scanning MITT before data processing; (b) the spectra of the signals from y = 20 mm (dashed) and y = 2 mm (solid).

To explain these problems, we resort to the relationship between the lateral resolution of the detecting ultrasonic transducer and the frequency spectrum of the received temporal waveform. The lateral resolution of the ultrasonic transducer is determined by its focal diameter, which is given by

$$d_f = \frac{1.02 v_a l_f}{d_a f_a}, \tag{1}$$

where v_a is the speed of sound in the medium, l_f is the focal length of the transducer, d_a is the diameter of the active element in the transducer, and f_a is the acoustic frequency. Therefore, the lateral resolution is inversely proportional to the frequency of the acoustic signal or the piezoelectric signal. Because the dominant frequency components of the piezo-electrical signals are far below 1 MHz, as shown in Fig. 2(b), the lateral resolution is much worse than the focal diameter of the transducer, 2 mm, at its 1-MHz central frequency.

Poor resolution that is caused by the dominating low-frequency components is also responsible for the ghost piezoelectric signals at y = 2 mm, where the transducer axis does not cross the buried muscle and thus the received piezoelectric signals can be only wide-angle low-frequency signals. In comparison, the piezoelectric signal at y = 20 mm—where the acoustic axis of the transducer crosses the muscle—is primarily from the transducer axis and hence has greater high-frequency components than the piezoelectric signal at y = 2 mm, as shown in Fig. 2(b).

From the above discussion, it is clear that increasing the high-frequency components of the piezoelectric signals can improve the lateral resolution. The most natural solution is to apply a bandpass filter to cut off the low-frequency components. An example of such processing, in which the filter has a passband between 0.5 and 1.5 MHz with a transition bandwidth of ~0.5 MHz, is shown in Fig. 3. The lateral resolution is much improved but still unsatisfactory; however, the axial resolution seems worse, and some artifacts were generated. The poor axial resolution is due to the decrease of bandwidth in the signal processing. As shown in Fig. 2(b), the spectral amplitude drops rapidly with the frequency; therefore, the filtered signal has a narrower bandwidth than the original one. A narrower bandwidth in the frequency domain results in a broader signal in the time domain thus poor axial resolution.

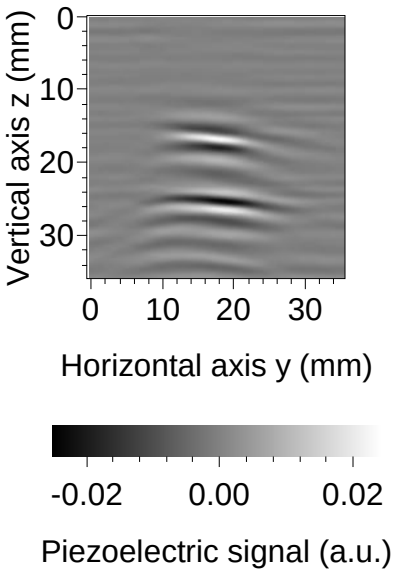

Fig. 3. The 2-D image after filtering the temporal signals with a standard bandpass filter.

To overcome the difficulties of the simple filtering, we proposed a reshaping method in the frequency domain. This method can make the bandwidth of the processed signal broader to enhance the axial resolution and weigh the high-frequency components more heavily to improve the lateral resolution. The essence of this method is to apply a self-adaptive filter to each temporal signal. The shape of the reshaping filter for the signal at y = 20 mm is chosen to be the inverse of the envelope of the original frequency spectrum(solid curve in Fig. 4); where the envelope of the spectrum is obtained by connecting the major local maxima, as shown by the dashed curve in Fig. 4. Without distorting the positions of the pulses in the temporal signal, this filter can achieve the widest possible bandwidth in the filtered signal and consequently the best axial resolution. Moreover, to filter out the very low-frequency disturbance—which is caused by the preamplifier—and the high-frequency noise beyond the cutoff frequency—where the signal-to-noise ratio is unity, a smoothing filter is applied to the signal. Unlike the self-adaptive reshaping filter, the smoothing filter is the same for the signals from all the scanned positions of the transducer.

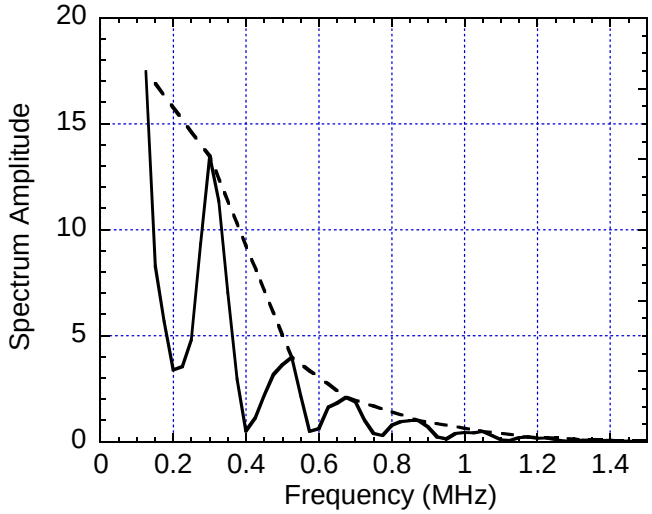

Fig. 4. The envelope (dashed curve) of the spectrum (solid curve) of the temporal signal at y = 20 mm.

The final filter is the product of the above two filters in the frequency domain. To increase the contrast, the background value is subtracted from the spectrum before applying the final filter. As we wish to obtain a lateral resolution

approaching that at 1.31 MHz, the final filter is scaled by a constant factor such that the spectral amplitude of the final filter at 1.31 MHz is set to unity; consequently, the spectral amplitudes of the piezoelectric signals for all piezoelectric signals remain unchanged at 1.31 MHz. The processed 2-D image (Fig. 5) is much clearer than the original image. The ghost objects in the original images were removed, and the two boundaries became quite distinct from the background. The muscle along the *y* axis in the image is about 15 mm, which agrees well with the 14-mm actual size.

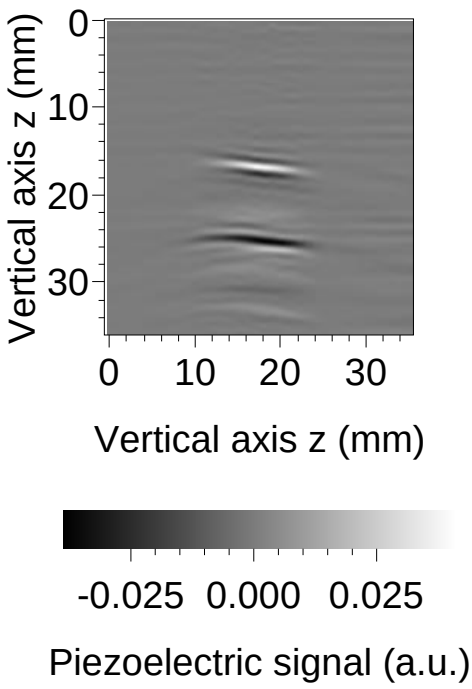

Fig. 5. The 2-D image after applying the final filter to the temporal piezoelectric signals.

In general, applying the reshaping filter will sharpen the boundaries of signals, which can be illustrated with an ideal slab. The thermoacoustic wave from a slab irradiated by a sufficiently short microwave pulse can be represented by a square wave. It can be shown that filtering the square wave with the reshaping filter is equivalent to taking the first derivative of the wave in the time domain, which yields the two boundaries of the slab. The spectral amplitude of the square wave with a duration a is $\left|\sin(\pi a f)/(\pi f)\right|$; thus its envelope is $1/(\pi f)$, and the reshaping filter is πf. Applying the reshaping filter to the square wave in the frequency domain is equivalent, within a constant factor, to differentiating the signal in the time domain, which yields a positive delta function at the front boundary of the square wave and a negative one at the rear boundary. More detailed discussion and some simulation results can be found in another paper from our group.[18]

Our study pointed out some potential approaches that can be used to improve the imaging resolution in our experiments. One approach is to improve the SNR of the signal so that the cutoff frequency is extended. Because only the spectral region with an SNR greater than unity provides useful information for our reshaping method, an increased cutoff frequency can broaden the usable spectrum and accordingly improve both the lateral and the axial resolutions. However, this advantage can only be realized when the spectrum is reshaped because the unprocessed high-frequency spectral amplitude is so small compared with the low-frequency one that it contributes little to improving the lateral and the axial resolutions, as shown in Fig. 2(b); after the reshaping, the weight of the high-frequency portion is increased greatly, resulting in an improved resolution. Another potential approach to improving the resolution is to shift the acoustic spectrum to a higher frequency by modulating the microwave source.

4. CONCLUSIONS

Our studies showed that scanning MITT is a promising imaging tool for biological tissues. The boundaries of different tissue constituents can be imaged clearly and accurately with the assistance of image processing. By reshaping the spectra of the piezoelectric signals, the weight of the high-frequency components is increased greatly, resulting in much improved axial and

lateral resolutions, both of which were 1 mm in our current experimental setup. Our spectral-reshaping method can also be applied to other ultrasonic signals comprising several pulses of similar shapes.

5. ACKNOWLEDGMENTS

We thank G. Ku for experimental assistance. This project was sponsored in part by the U.S. Army Medical Research and Materiel Command Grant No. DAMD17-00-1-0455, the National Institutes of Health Grants No. R01 CA71980 and No. R21 CA83760, the National Science Foudation Grant No. BES-9734491, and Texas Higher Education Coordinating Board Grant No. ARP 000512-0123-1999.

6. REFERENCES

1 W. Joines, R. Jirtle, M. Rafal, and D. Schaeffer, "Microwave power absorption differences between normal and malignant tissue," Radiation Oncology-Biology-Physics 6, 681–687 (1980).
2 S. Chaudhary, R. Mishra, A. Swarup, and J. Thomas, "Dielectric properties of normal human breast tissues at radiowave and microwave frequencies," Indian Journal of Biochemistry and Biophysics 21, 76–79 (1984).
3 W. Joines, Y. Zhang, C. Li, and R. Jirtle, "The measured electrical properties of normal and malignant human tissues from 50–900 MHz," Medical Physics 21, 547–550 (1994).
4 L. E. Larsen and J. H. Jacobi, eds., Medical Applications of Microwave Imaging (IEEE Press, Piscataway, NJ, 1986).
5 S. Caorsi, A. Frattoni, G. L. Gragnani, E. Nortino, and M. Pastorino, "Numerical algorithm for dielectric-permittivity microwave imaging of inhomogeneous biological bodies," Med. Biol. Eng. Comput. 29, NS37–44 (1991).
6 M. S. Hawley, A. Broquetas, L. Jofre, J. C. Bolomey, and G. Gaboriaud, "Microwave imaging of tissue blood content changes," J. Biomed. Eng. 13, 197–202 (1991).
7 P. M. Meaney, K. D. Paulsen, and J. T. Chang, "Near-field microwave imaging of biologically-based materials using a monopole transceiver system," IEEE Trans. Microwave Theory Tech. 46, 31–45 (1998).
8 R. A. Kruger, P. Liu, Y. R. Fang, and C. R. Appledorn, "Photoacoustic ultrasound (PAUS)—reconstruction tomography," Med. Phys. 22, 1605–1609 (1995).
9 C. G. A. Hoelen, F. F. M. Demul, R. Pongers, and A. Dekker, "Three-dimensional photoacoustic imaging of blood vessels in tissue," Opt. Lett. 23, 648–650 (1998).
10 A. A. Karabutov, E. V. Savateeva, N. B. Podymova, and A. A. Oraevsky, "Backward mode detection of laser-induced wide-band ultrasonic transients with optoacoustic transducer," J. of Appl. Phys. 87, 2003–2014 (2000).
11 T. Bowen, L. Nasoni, A. E. Pifer, and G. H. Sembrosk, "Some experimental results on the thermoacoustic imaging of soft tissue -equivalent phantoms," Proc. IEEE Ultrasonics Symposium 2, 823–827 (1981).
12 R. G. Olsen and J. C. Lin, "Acoustic imaging of a model of a human hand using pulsed microwave irradiation," Bioelectromagnetics 4, 397–400 (1983).
13 J. C. Lin and K. H. Chan, "Microwave thermoelastic tissue imaging—system design," IEEE Trans. Microwave Theory Tech. 32, 854–860 (1984).
14 R. A. Kruger, D. R. Reinecke, and G. A. Kruger, "Thermoacoustic computed tomography—technical considerations," Med. Phys. 26, 1832–1837 (1999).
15 L.-H. V. Wang, X. Zhao, H. Sun, and G. Ku, "Microwave-induced acoustic imaging of biological tissues," Rev. Sci. Instrum. 70, 3744–3748 (1999).
16 G. Ku and L.-H. V. Wang, "Scanning thermoacoustic tomography in biological tissue," Med. Phys. 27, 1195–1202 (2000).
17 G. Ku and L.-H. V. Wang, "Scanning microwave-induced thermoacoustic tomography: signal, resolution, and contrast," Medical Physics, in press (2001).
18 Y. Xu and L.-H. V. Wang, "Signal procession in scanning thermoacoustic tomography in biological tissue", submitted to Medical Physics.